31st Congress of the International Council of the Aeronautical Sciences

Belo Horizonte, Brazil; September 09-14, 2018

AERODYNAMIC DESIGN OF A RIGID COAXIAL ROTOR AIRFOIL IN UNSTEADY FLOW

Xudong Yang*, Ming Huang*
***Northwestern Polytechnical University**

Keywords: *Aerodynamic Design, Rigid Coaxial Rotor, Efficient Global Multi-point Optimization, Unsteady Flow*

Abstract

High-speed helicopter (Flight speed ≥ 400km/h) with rigid coaxial rotor, which is based on Advanced Blade Concept (ABC), gains more and more attention. Double-ended airfoils are introduced to decrease the drag and noise caused by root segment of coaxial rotors in reverse flow. In this paper, the design of a double-ended airfoil is conducted by an efficient global multi-objective optimization method. The baseline is DBLN526. Compared with the baseline, drag coefficient of designed airfoils can be reduced up to 19.89%, lift-to-drag ratio can be raised up to 17.31%. The characteristics in unsteady flow improve to some extent.

1 General Introduction

Rigid coaxial rotor is one of the most promising configuration for helicopter which is able to land/take off vertically, as well as cruise in a high speed. This kind of rotor is based on the Advancing Blade Concept(ABC), which is distinguished with conventional rotor, mainly for the lift-offset and the unloaded retreating blades. The concept makes full use of the two advancing blades, whereas the retreating blades, especially the root segment, are left in deeply reverse flow, causing severe drag and noise problem. Double-ended airfoil are introduced to handle these problem in the design of the famous demonstrator of Sikorsky, X2TD. In the disclosed Sikorsky airfoil library, the airfoil conforming to the profile of the X2TD with weak separation airfoil is the DBLN526.

The DBLN526 airfoil is a bilateral symmetric airfoil with a large thickness of 26% and a blunt trailing edge. There is a slight abrupt change in the curvature of the lower surface. According to the experimental results of the free transition of the NF-3 low-speed airfoil wind tunnel of Northwestern Polytechnical University, as shown in Fig. 1, the laminar flow area can be maintained to 50% of the chord length when the angle of attack(AoA) increases to 5 degrees. Therefore, the transition simulation plays an important role in understanding the flow mechanism of the airfoil and aerodynamic design of the airfoil.

The large thickness and the blunt trailing edge usually mean that flow separation is likely to occur at the trailing edge of the airfoil. In this paper, the static and dynamic characteristics of the DBLN526 airfoil are numerically simulated using the RANS-based solver. It can be seen from the figures that there are different levels of separation at different trailing edge.

The double-ended airfoil is located within 0.35R of the rigid coaxial blade and the chord length is approximately 0.25m. According to the velocity distribution along the span when X2TD in forward flight and hover, the minimum forward flow Mach number over DBLN526 is about 0.2, while the maximum is about 0.55. And the maximum reverse flow Mach number is 0.22. In order to improve cruising efficiency and high-speed performance, it is important to decrease the drag coefficient at medium AoA when the Mach number of forward flow is between 0.3 – 0.5, and decrease the drag coefficient in reverse flow while reducing flow separation.

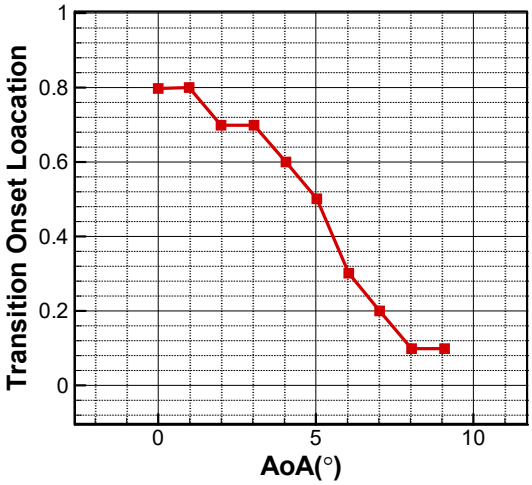

Fig. 1 Transition position of DBLN526 in different AoA

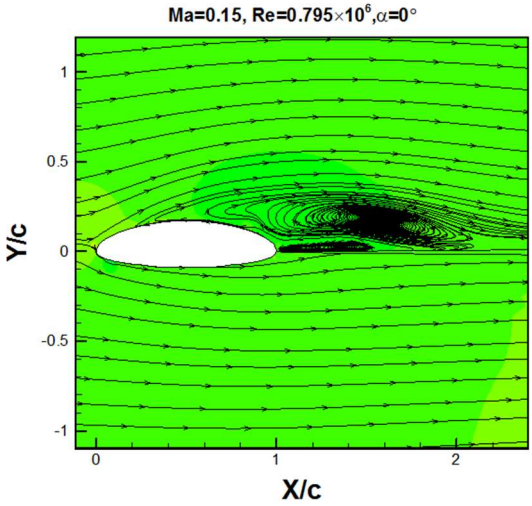

Fig. 2 Streamline of DBLN526, calculated by RANS with full turbulence

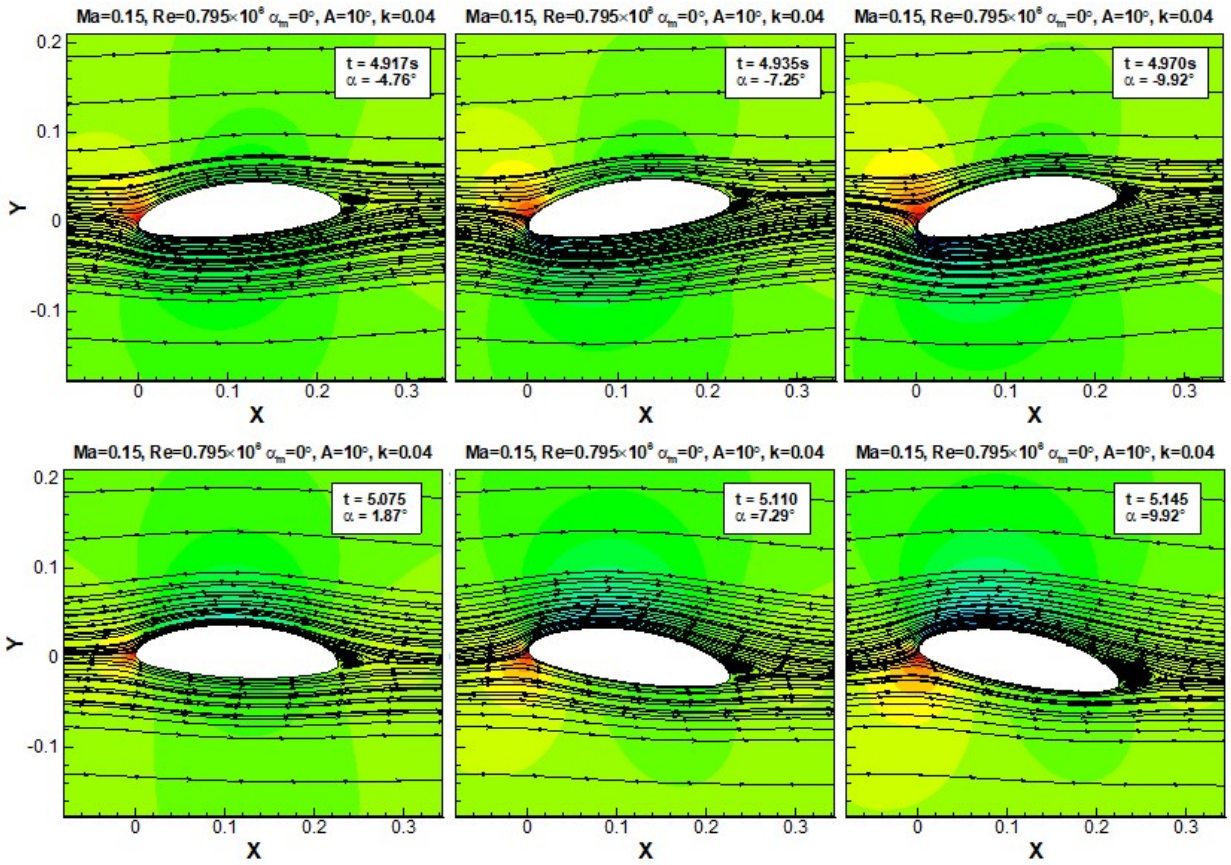

Fig. 3 Streamline of DBLN526 in different momentCalculated by unsteady RANS with full turbulence

2 Aerodynamic Design Method

2.1 Airfoil Parameterization Method and Flow Solver

In this paper, two sorts of parameterization methods are used to describe the perturbations of new airfoils. Class function / Shape function Transformation (CST) is used for bilateral asymmetric design, with 6 design variables on upper surface and lower surface respectively, and Free Form Deformation (FFD) is used for bilateral symmetric design with 5 design variables on upper surface and lower surface respectively.

The aerodynamic characteristics of airfoils are solved by XFOIL. XFOIL is a software developed by Prof. Mark Drela of MIT for low and subsonic airfoil calculation and design. Fig. 4 and Fig. 5 shows the compare of aerodynamic analysis results and experimental data of the DBLN526 airfoil. The calculation results are from XFoil free transition (e^N), ANSYS FLUENT free transition (using transition model) and full turbulence calculation (using SST turbulence model). The experimental data are from the NF-3 low-velocity airfoil wind tunnel of the Northwestern Polytechnical University. The Ma number is 0.069, Reynolds number is 0.8×10^6. Comparing the curves in the figure, we can see that for the lift coefficient calculation, the result of XFOIL is slightly larger than the experimental value, and ANSYS FLUENT using transition model is slightly smaller; For drag efficient calculations, XFOIL is in better agreement with the experimental values. Regardless of whether it is lift or drag coefficient, the full turbulence calculation based on RANS is far from the experimental value. This shows that the laminar flow in the airfoil flow plays an important role, and it is not reliable to perform pure turbulence analysis.

The calculation results show that the XFOIL prediction results for the blunt trailing edge double ended airfoil drag coefficient are reliable.

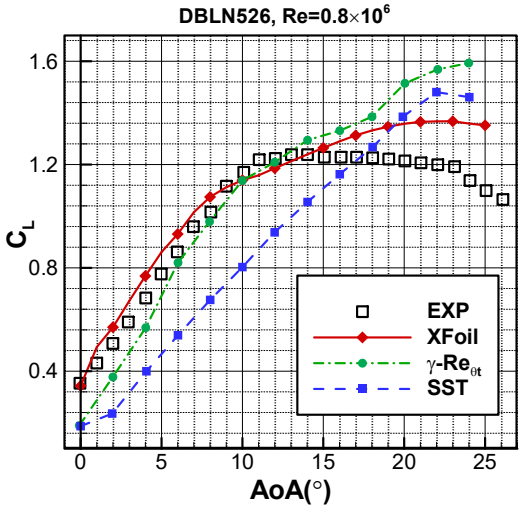

Fig. 4 Ma=0.069, Re=0.8×10^6, C_L varying with AoA

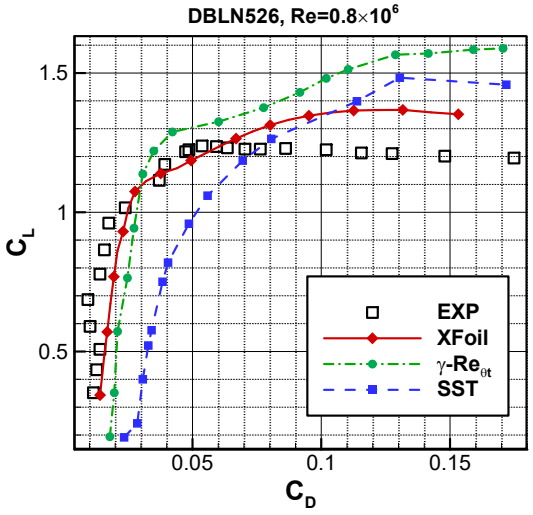

Fig. 5 Ma=0.069, Re=0.8×10^6, C_L varying with C_d

2.3 Efficient Global Multi-Objective Optimization Method based on Hypervolume and Kriging Model

In this paper, an efficient global multi-objective method based on hypervolume indicator (HVI) and kriging is used for the design optimization.

The process of the method is shown as Fig. 6. In order to verify the effectiveness of the proposed method, a numerical example of multi-objective numerical optimization is conducted. And the method is compared with the classic multi-objective optimization method NSGA-II and some other infilling criterion. The objective function is as follows.

$$\min.\ f_1(x_1,x_2,x_3)=\sum_{i=1}^{2}\left[-10\exp\left(-0.2\sqrt{x_i^2+x_{i+1}^2}\right)\right]$$
$$f_2(x_1,x_2,x_3)=\sum_{i=1}^{3}\left[|x_i|^{0.8}+5\sin x_i^3\right] \quad (1)$$
$$s.t.\quad -5\le x_i\le 5,\ i=1,2,3$$

The results are shown as Fig. 7 and Fig. 8 It can be seen that the optimization method used in this paper has a relatively balanced global search and local search capability.

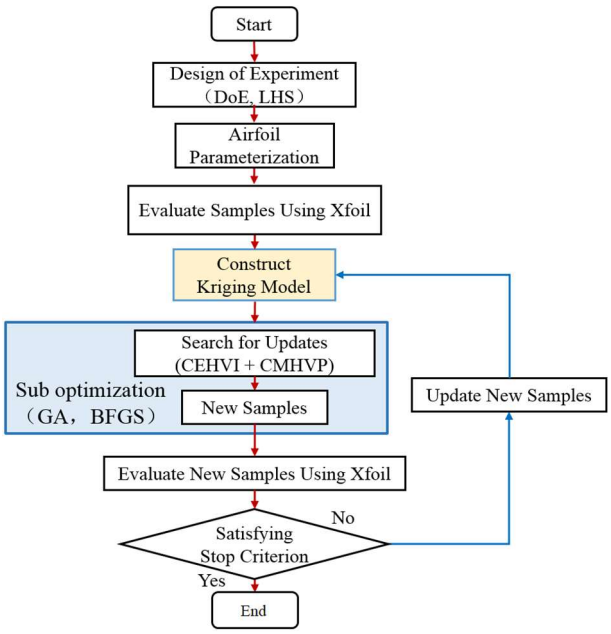

Fig. 6 Process of Efficient Global Multi-Objective Optimization

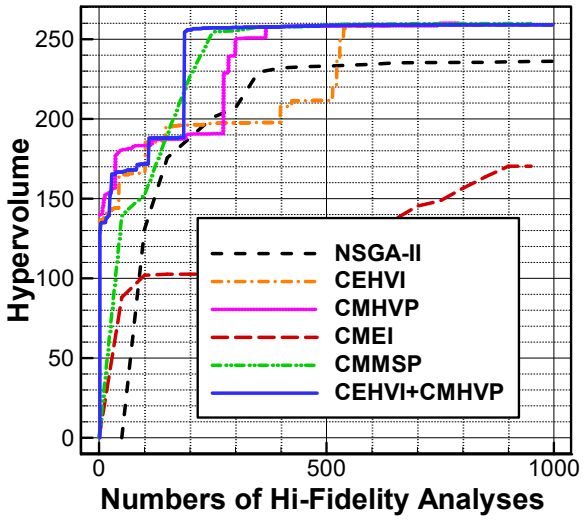

Fig. 7 Comparison of HVI Convergence

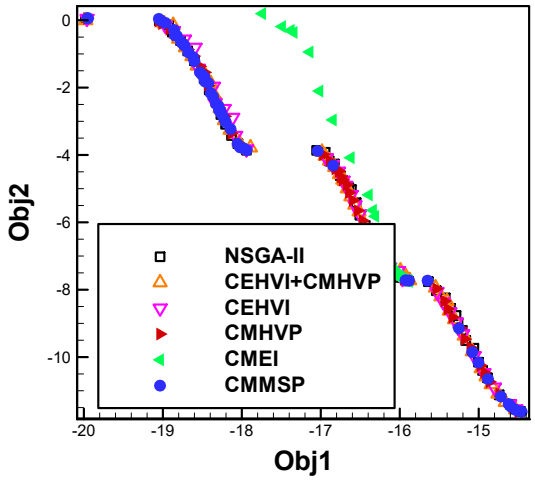

Fig. 8 Comparison of Optimization Result

3 DBLN526 Airfoil Optimization

The flow field of DBLN526 has the characteristics of large laminar flow range, strong flow separation at the trailing edge, and so on, which puts forward higher requirements for the unsteady performance of the airfoil. High fidelity unsteady CFD is too time-consuming, in order to decrease computing cost, this paper conducts a multi-point optimization design under uniform inflow conditions, and the unsteady performances of the optimized airfoil under non-uniform inflow conditions are analyzed.

3.2 Optimization Model

The design points and objectives are shown in the following table. In order to ensure the overall aerodynamic characteristics of a coaxial rigid rotor, several key aerodynamic characteristics were selected as calibration indicators.

Superscripts in the table indicate design points. *a* is an undetermined coefficient, and the specific value needs to fully consider the characteristics of the blade structure and the overall objective of the helicopter to make corresponding adjustments. In general, the bigger the *a* is, the looser the torque constraint is, and the drag coefficient of optimized airfoil is usually smaller. However, the torque coefficient can be larger.

Tab. 1 Design Points and Flow Conditions

Design Point	Flow Condition
1	$Ma=0.3,\ \mathrm{Re}=1.65\times10^6,\ \alpha=7°$
2	$Ma=0.4,\ \mathrm{Re}=2.2\times10^6,\ \alpha=5°$
3	$Ma=0.5,\ \mathrm{Re}=2.75\times10^6,\ \alpha=3°$
4	$Ma=0.2,\ \mathrm{Re}=1.1\times10^6,\ C_L=0.6$
5	$Ma=0.3,\ \mathrm{Re}=1.65\times10^6,\ C_L=0.6$
6	$Ma=0.55, Cl=0$

Tab. 2 Objects and Constraints

Object	Constraint
Decrease C_d^1	$\left\|C_m^1\right\|(\text{design}) \le a^1 \cdot \left\|C_m^1\right\|(DBLN526)$
Decrease C_d^2	$\left\|C_m^2\right\|(\text{design}) \le a^2 \cdot \left\|C_m^2\right\|(DBLN526)$
Decrease C_d^3	$\left\|C_m^3\right\|(\text{design}) \le a^3 \cdot \left\|C_m^3\right\|(DBLN526)$
Increase K^4	$\left\|C_m^6\right\|(\text{design}) \le a^6 \cdot \left\|C_m^6\right\|(DBLN526)$
Increase K^5	$Area \ge Area_{baseline}$
Decrease C_{d0}^6	$Thickness \ge Thickness_{baseline}$

Tab. 3 Calibration Indicators

Flow Condition	Calibration Indicator
$Ma=0.2,\ \alpha=180°$	C_d
$Ma=0.3,\ \mathrm{Re}=1.65\times10^6$	$K_{\max}$
$Ma=0.4,\ \mathrm{Re}=2.2\times10^6$	$K_{\max}$
$Ma=0.5,\ \mathrm{Re}=2.75\times10^6$	$K_{\max}$

Taking into account the calculation cost and optimization efficiency, the following optimization models are proposed:

$$
\begin{aligned}
&Obj. \quad \min.\ F_{obj}\\
&F_{obj}(1)=0.25\times\frac{C_d^1}{0.001}+0.3\times\frac{C_d^2}{0.001}+0.35\times\frac{C_d^3}{0.001}+0.1\times\frac{C_d^6}{0.001}\\
&F_{obj}(2)=0.5K^4+0.5K^5\\
&s.t. \quad \left|C_m^1\right|(\text{design}) \le a^1 \cdot \left|C_m^1\right|(DBLN526)\\
&\left|C_m^2\right|(\text{design}) \le a^2 \cdot \left|C_m^2\right|(DBLN526)\\
&\left|C_m^3\right|(\text{design}) \le a^3 \cdot \left|C_m^3\right|(DBLN526)\\
&\left|C_m^6\right|(\text{design}) \le a^6 \cdot \left|C_m^6\right|(DBLN526)\\
&Area \ge Area_{baseline}\\
&Thickness \ge Thickness_{baseline}
\end{aligned}
$$

3.2 Optimization Results

Considering the particularity of the shape of DBLN526, this paper has adopted two different design schemes and studied the performance improvement brought by different design schemes.

The first scheme is bilateral asymmetric optimization scheme under uniform flow conditions, focusing on increasing lift-to-drag ratio to improve hover and forward flight efficiency. The idea comes from the analysis of the characteristics of the flow around the rotor of X2TD. When X2TD moves forward at Mach number 0.3, the ratio of positive to negative flow pressures of approximately 9:1. Therefore the optimized airfoil should be bilateral asymmetric.

However, due to the fact that the existing investigations and calculations have not clearly illustrated the specificity of the DBLN 526 shape, this section proposes a second optimization in order to explore the effect of maintaining or amplifying the original shape characteristics of the original airfoil on the airfoil performance, which is symmetrical airfoil design under uniform flow conditions, exploring the influence of abrupt changes in surface curvature on airfoil performance.

3.2.1 Shape of Bilateral Asymmetric Design

The results of the two optimizations are compared with the baseline, and the airfoil shape comparison is shown in the Fig. 9.

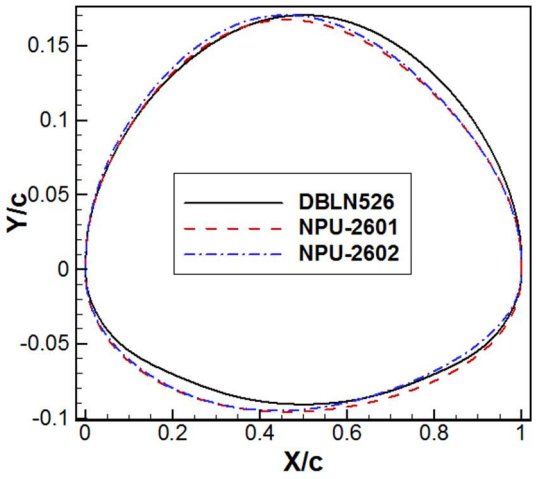

Fig. 9 Shape Comparison Between Baseline and Optimized Airfoil

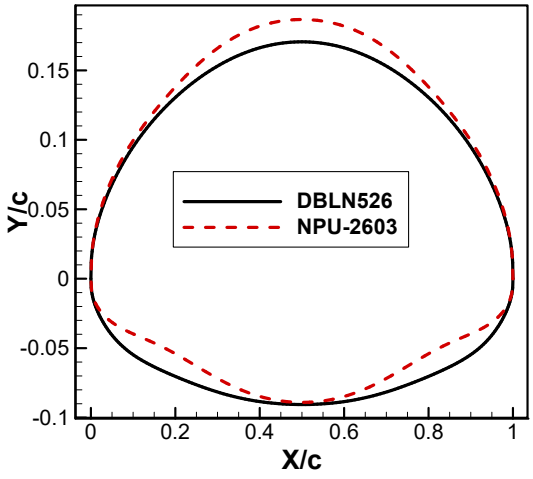

Fig. 10 Shape Comparison Between Baseline and Optimized Airfoil

The radius of the leading edge of the optimized airfoil is all increased. The increase in bluntness is conducive to maintaining trailing edge stall and increasing the laminar flow range during positive flow. The maximum camber decreases and the maximum camber position moves forward, which helps to further reduce drag coefficient in positive flow; NPU-2601 has a slightly larger radius at the trailing edge than NPU-2602. The aerodynamic characteristics in steady and unsteady flow will be discussed chapter 3.2.3 and 3.2.4

3.2.2 Shape of Bilateral Asymmetric Design

To facilitate symmetric control, the optimization uses FFD parameterization. The airfoil is divided into two parts in accordance with the axis of symmetry. Five control points are selected on upper and lower surface respectively to control the left side. There are a total of 10 variables, and the right half of the control point information is the same as the left half. The shape of optimized airfoil and baseline are shown in the Fig. 9.

The maximum thickness of the optimized airfoil is significantly increased, which is beneficial to the structural characteristics. The inward depression of the lower surface is more pronounced than the baseline. The aerodynamic characteristics in steady and unsteady flow will be discussed chapter 3.2.3 and 3.2.4

3.2.3 Aerodynamic characteristics in steady flow

The following table shows the comparison of the aerodynamic characteristics of optimized airfoils and baseline. (Using Xfoil free transition analysis).

As can be seen from the following table, NPU-2601 has a higher lift-to-drag ratio than baseline airfoil at a higher Mach number, which helps to improve helicopter hovering and forward flight efficiency; however, poor torque characteristics can cause larger operating load in forward flight. Then stricter torque constraints and increased design space were used for the second design, which was named NPU-2602. The comparison between NPU-2602, NPU-2601 and baseline shows that NPU-2602 has better lift and drag characteristics at Mach 0.3-0.5, and the torque characteristics have been improved. However, compared with the baseline, NPU-2601 and NPU-2602 have a slight increase in the drag coefficient under Mach 0.55, which is not conducive to the high-speed flight of helicopters. This is because of the selection of the ratio of weight coefficients for forward and reverse flow at high-speed forward flight, the optimization process chose to greatly improve the forward flow characteristics with a slight sacrifice of the reverse flow characteristics. For NPU-2603, the main design goals under the six design points have been improved, the drag coefficient can be reduced by up to 20.88%, and the lift-to-drag ratio is increased by up to 19.94%; all constraints are fulfilled, but the

torque coefficient as active constraint is reduced by 60%. -70% may be due to the fact that the airfoil lift-drag ratio still has a large potential for improvement or the selection of the optimization model weight coefficient is unreasonable, and further design studies are needed.

Tab. 4 Comparison of Aerodynamic Characteristics of Optimized Airfoil and Baseline

		DBLN526	NPU-2601	Δ(%)	NPU-2602	Δ(%)	NPU-2603	Δ(%)
Objectives	Cd^1	0.02519	0.02233	-11.35%	0.02042	-18.94%	0.02234	-11.31%
	Cd^2	0.02132	0.01930	-9.47%	0.01708	-19.89%	0.01853	-13.09%
	Cd^3	0.02165	0.01908	-11.87%	0.01761	-18.66%	0.01713	-20.88%
	K^4	35.31	36.87	4.42%	40.39	14.39%	42.29	19.77%
	K^5	34.55	37.46	8.42%	40.53	17.31%	41.44	19.94%
	$Cd0^6$	0.01624	0.01511	-6.96%	0.01403	-13.61%	0.01612	-0.74%
constrains	$\lvert C_m^1 \rvert$	0.0470	0.0635	35.11%	0.0377	-19.79%	0.01758	-62.60%
	$\lvert C_m^2 \rvert$	0.0533	0.0550	3.19%	0.0317	-40.53%	0.01419	-73.38%
	$\lvert C_m^3 \rvert$	0.0457	0.0364	-20.35%	0.0199	-56.46%	0.01301	-71.53%
	Area	0.2007	0.2015	0.40%	0.2009	0.10%	0.2011	0.20%
	Thickness	0.261	0.263	0.77%	0.265	1.53%	0.2757	5.63%
Calibration Indicator	$Cd_{Ma=0.2,\ \alpha=180°}$	0.01395	0.01518	8.82%	0.01642	17.71%	0.01373	-1.58%
	$K_{\max\lvert Ma=0.3}$	38.0049	46.3319	21.91%	45.4918	19.70%	44.8596	18.04%
	$K_{\max\lvert Ma=0.4}$	35.881	43.4348	21.05%	42.8291	19.36%	40.1153	11.80%
	$K_{\max\lvert Ma=0.5}$	35.2593	41.723	18.33%	40.4551	14.74%	32.9368	-6.59%

3.2.4 Aerodynamic characteristics in unsteady flow

The
Tab. **4** shows the comparison of the aerodynamic characteristics of optimized airfoils and baseline. (Using Xfoil free transition analysis).

This paper takes the X2TD rotor as an example to analyze the unsteady performance of the above designed airfoil assembled on the X2TD rotor. The X2TD rotor has a chord length of 0.24 meters, maximum Mach number of rotor tips in forward flight is 0.88, and a paddle radius of 4 meters. For a rigid-coaxial rotor, the flapping amplitude is small, so the following analysis ignores the flapping motion and considers only the coupling of pitch and back-and-forth motion of the airfoil. Regardless of the trimming problem, the amplitude of the angle of attack is:

$$Ma = Ma_0 - 0.2\sin(\omega t)$$

$$\alpha = \alpha_0 + 4.0 \times \sin(\omega t)$$

According to [6], the maximum Mach number at the tip of the rotor is set to 0.88. The double-ended airfoil is used at 0.55R. According to the distribution of the blade radial velocity, the mean Mach number is 0.238, the average angle of attack is 4°, and the reduction frequency k=0.0857. O-grid is used, with the number of grid cells being approximately

60,000, and the first-layer grid height being 1×10^{-6}, 50 times far field. The solver is FLUENT, which adopts dynamic grid technology and adaptive time stepping technology. Each cycle has a maximum of 3000 time steps, and the maximum number of iterations of pseudo-time is 200 times. A total of 3-5 cycles are calculated. The final convergence and periodicity are good. Fig. 5 30 - Fig. 5 32 respectively show the airfoil lift, drag and moment coefficients as a function of angle of attack before and after optimization.

Under dynamic conditions, the drag coefficient and torque coefficient hysteresis curves of NPU-2602 are better than those of the baseline, the time-average lift coefficient is slightly lower, but the area of the hysteresis curve of lift decreases, overall the optimized airfoil meets the design requirements. At the same time, it can be seen that there is a certain correlation between the unsteady aerodynamic characteristics and the steady characteristics of the airfoil before and after optimization. For example, the torque characteristics of NPU-2602 under steady flow is better than that of NPU-2601, and the dynamic characteristics of its torque coefficient are also improved, the average moment coefficient decreases. However, the limitations of steady-state optimization are also obvious. For example, in the steady-state design, although the main aerodynamic performance of the NPU-2603 at the design point is better than that of the basic airfoil, the dynamic characteristics are even inferior to baseline, in terms of the time-averaged aerodynamic force or the aerodynamic force. The hysteresis curve area is inferior to the reference airfoil. In addition, the presence of a certain range of negative resistance areas under dynamic conditions may be due to the separation of detached vortexes and appendages.

Due to the lack of experimental verification, and the numerical calculation method based on RANS has a large dissipation of vortices, it is impossible to accurately capture the vortex generation and development process. Therefore, further research is needed.

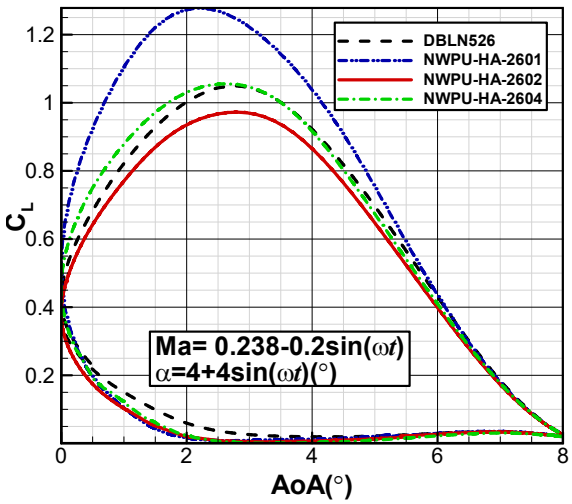

Fig. 11 Comparison of Hysteresis Curve of Lift Coefficient between Optimized Airfoil and Baseline

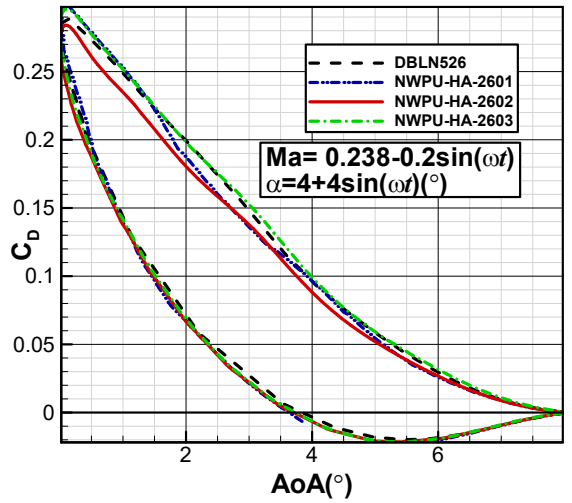

Fig. 12 Comparison of Hysteresis Curve of Drag Coefficient between Optimized Airfoil and Baseline

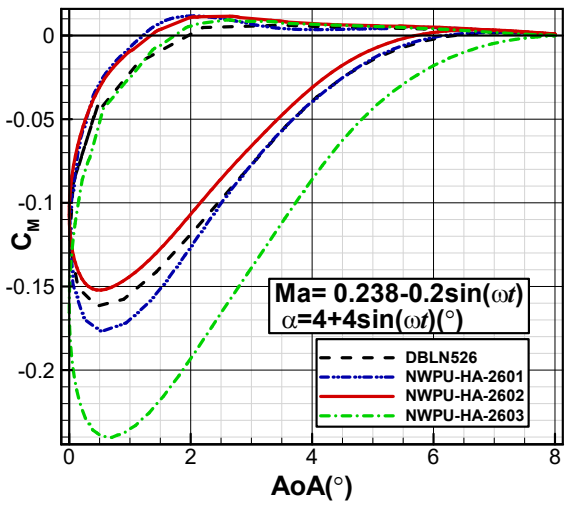

Fig. 13 Comparison of Hysteresis Curve of Moment Coefficient between Optimized Airfoil and Baseline

4 Conclusions

1. According to the experimental and analytical results, laminar flow and flow separation play important roles in the flow over DBLN526. Therefore, the simulations on transition and separation are essential to understand the flow mechanism of the airfoil and aerodynamic design of the airfoil

2. Under the uniform inflow conditions, the eva-luation results show that the main characteristics of the optimized airfoil under design points have been improved, and the optimization results meet the design requirements. Compared with the baseline, drag coefficient of designed airfoils can be reduced up to 19.89%, lift-to-drag ratio can be raised up to 17.31%. The characteristics in unsteady flow are improved to some extent. The asymmetric design shows disadvantage in unsteady flow, and further research is needed to enclose the mechanism of this phenomenon.

3. Good performances in multi-points generally mean good ones in unsteady flow. However, it is exceptional for symmetrical design, which is to be understood in further research.

References

[1] Andrew H. L., Jonathan N. L., Anya R. J. Experimental Investigation of Reverse Flow over Sharp and Blunt Trailing Edge Airfoils. *31st AIAA Applied Aerodynamics Conference*, 2013.

[2] Bradley P., Ananth S., James B.. Computational investigation of coaxial rotor interactional aerodynamics in steady forward flight. *33rd AIAA Applied Aerodynamics Conference*, 2015.

[3] M. Emmerich, A. H. Deutz, J. W. Klinkenberg. Hypervolume-based expected improvement: monotonicity properties and exact computation. *Evolutionary Computation (CEC), IEEE Congress*, 2011.

[4] K. Deb, L. Thiele, M. Laumanns et al. Scalable test problems for evolutionary multi-objective optimziation. *Piscataway* 2002.

[5] Warwick, Graham, Sikorsky conducts first flight of S-97 helo. *Aviation Week & Space Technology*. 2015.

[6] Ashish Bagai. Aerodynamic of the X2 technology demonstrator main rotor blade. *Annual Forum of the American Helicopter Society*, 2008.

Contact Author Email Address

xdyang@nwpu.edu.cn

Copyright Statement